Chapter 5

Experimental Study

5.1 Introduction

In this chapter the laboratory tests on two reduced-scale steel structures are described: (1) a single-story model equipped with two FDs (SSMFD) and (2) a two-story building with a pair of FDs in each floor (TSMFD). The two tested models are described and their dynamic properties are described. The FD used in the tests is described too. The dynamic tests and the results obtained are also shown. Finally, a comparison between experimental and numerical (using ALMA) responses is discussed. A complete description of the installation and equipment used in the tests is included in Appendix D and the complete series of results is presented in Appendix E.

5.2 Scale Models

5.2.1 Description

The dimensions of the two rigs are shown in Figs. 5.1a and b. The structures are symmetric and composed of two moment resistant frames at each side along the X direction. The frame members are standard hollow sections of grade 43 structural steel. The member sections of both models are shown in Fig. 5.1c. The columns were designed to withstand a compressive axial load of 10.80 kN while the beams supported such load distributed along their length, assuming hinged connections at their ends. Only X motion was of interest. Since all joints are considered rigid in the calculations, they were properly welded. In Figs. 5.2a and b the actual tested models are shown. In order to get moment-resistant supports, both models were fixed to the shaking table by means of clamp-bolted connections along their lower horizontal members (see Fig. 5.2a). Some details of the connections are shown in Fig. 5.2c and d.

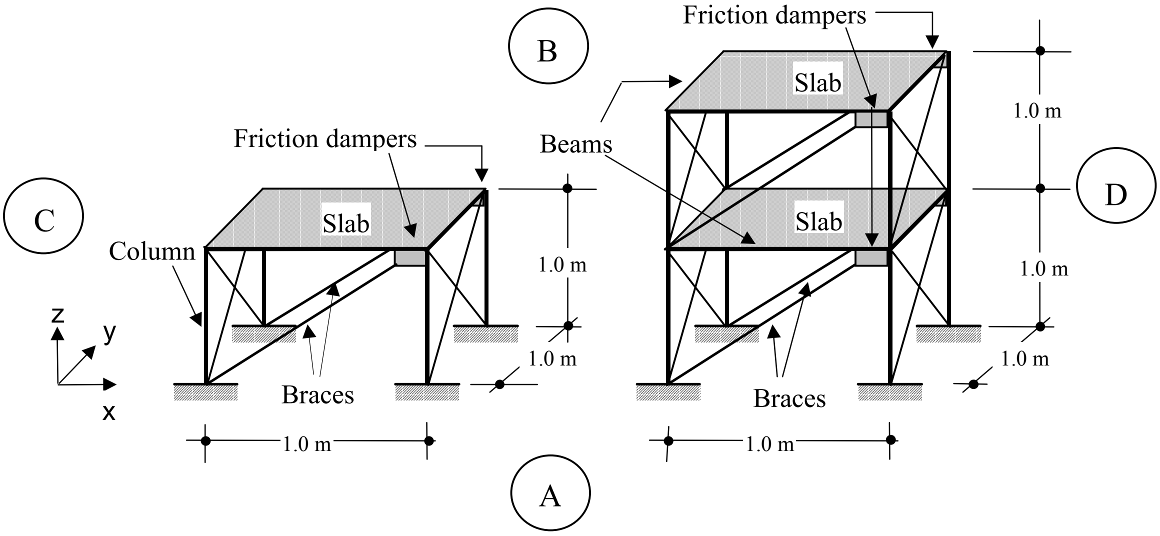

(a) Single-story model (SSMFD) (b) Two-story model (TSMFD)

Element	Face	Section	Steel
Column	A, B, C, D	SHS 4 × 4 × 0.30 cm	Grade 43
Beam	A, B, C, D	SHS 4 × 4 × 0.30 cm	Grade 43
Brace	A, B	CHS 2.69 × 0.32 cm	Grade 43
Brace	C, D	2.5 × 0.3 cm Rect. bar	Grade 43

(c) Member properties

Figure 5.1 Member properties of the tested scale-models

(a) Single-story model

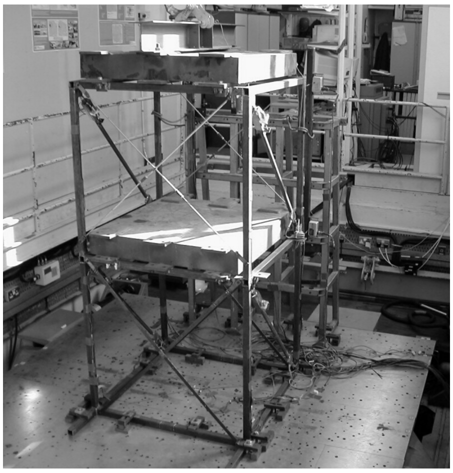

(b) Two-story model

(c) Hinged connection between a brace and the main frame

(d) Connection between the brace and the FD

Figure 5.2 Scale models and connections

5.2.2 Determination of the dynamic parameters of the rigs

5.2.2.1 Structural model

The structures are symmetric, thus their horizontal vibrations are described by discrete models (lumped masses) with one DOF per floor. Since only the motion in the X direction is considered, the SSM —bare frame— is represented by a SDOF model, while the TSM —bare frame— is respresented by a two DOF model (see Figs. 5.2 and 5.3). The setting of FDs in both models adds additional DOFs (see Chapters 3 and 4).

5.2.2.2 Bare frame masses

The masses were measured by means of a scale. The mass of the first floor is equal to 1067 kg, and the mass on top of the second floor is equal to 1105 kg. The halves of these values were used for the calculations as a single frame (front or rear) is considered. Hence, for the SSM, $m = 533.5$ kg and for the TSM, $m_1 = 533.5$ kg and $m_2 = 552.5$ kg: $\mathbf{M}^{ss} = \begin{bmatrix} 533.5 & 0 \\ 0 & 552.5 \end{bmatrix}$ kg.

5.2.2.3 Bare frame stiffness coefficients

The stiffness parameters of both bare frames were obtained from theoretical considerations assuming rigid connections and neglecting the contribution of the masses.

Figs. 5.3 and 5.4 show a schematic static test aimed to validate the numerical stiffness of the bare frames. For example, for the SSM, different values of the load P and the displacement x of the rigid slab, were registered (see Fig. 5.3b). Numerically, the values of displacement x were determined applying

$$x = \frac{P}{k} \tag{5.1}$$

where k is the stiffness of the frame. This value is calculated with the following expression

$$k = \frac{84EI}{5H^3} \tag{5.2}$$

where $E = 200$ GPa, $I = I_b = I_c = 9.96$ cm^4, and $H = 100$ cm. Eq. (5.2) considers both bending and joint rotation effects. With the aforementioned values $k = 334.597$ kN/m.

Table 5.1 shows the comparison between the values of the displacement x obtained experimentally and numerically with Eq. (5.1) for different values of P. The accuracy is found to be acceptable.

For the TSM, the stiffness matrix (bare frame), $\mathbf{K}^{ss}$, is obtained by theoretical considerations:

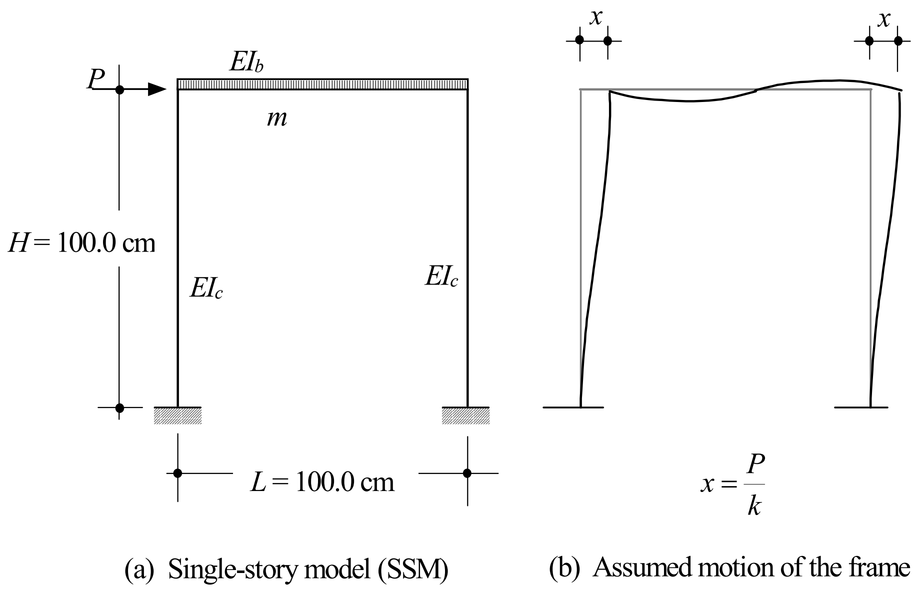

Figure 5.3 Static test made to determine stiffness of the SSM

Applied force P (N)	Displacement x (cm)	
	Experimental (average)	Numerical
490.35	0.160	0.147
980.70	0.315	0.293
1471.05	0.485	0.440

Table 5.1 Lateral displacement of SSM in the static test

Applied force P_1 (N)	Displacement x_1 (cm)		Displacement x_2 (cm)	
	Experimental (average)	Numerical	Experimental (average)	Numerical
490.35	0.165	0.142	0.200	0.187
980.70	0.330	0.284	0.410	0.373
1471.05	0.510	0.425	0.625	0.560

Table 5.2 Lateral displacement of the TSM in the static test

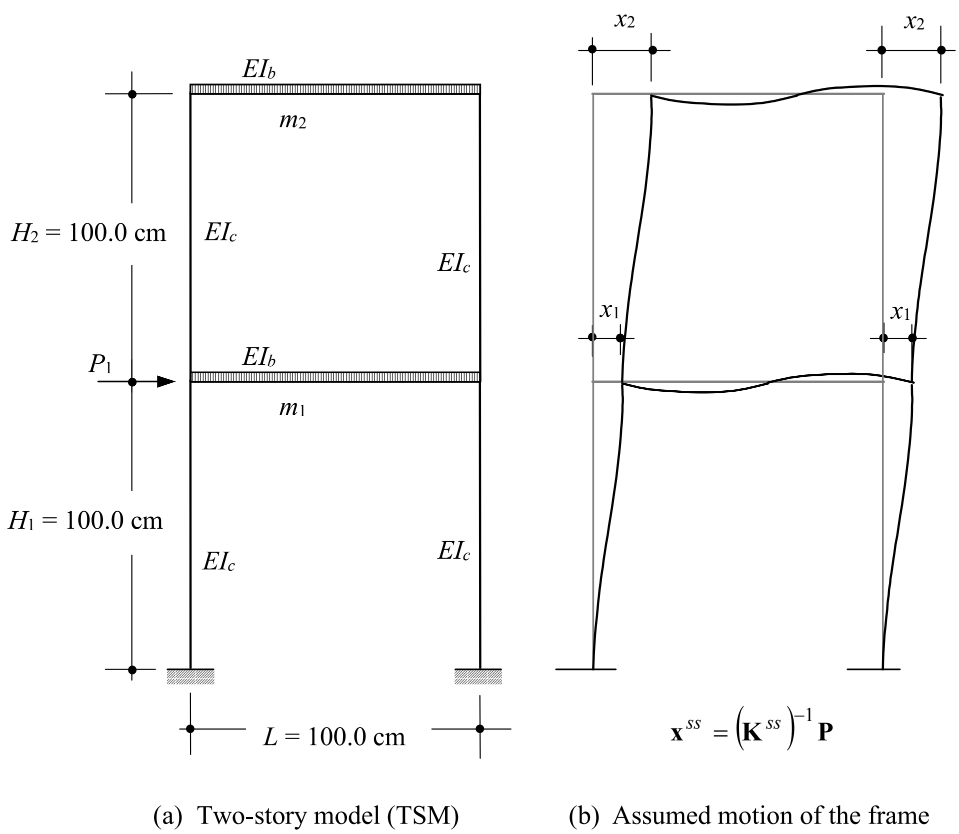

Figure 5.4 Static test made to determine the stiffness matrix of the TSM

$$\mathbf{K}^{ss} = \frac{EI}{17H^3}\begin{bmatrix} 690 & -300 \\ -300 & 228 \end{bmatrix} \tag{5.3}$$

Again, in Eq. (5.3) bending and joint rotation effects are considered. Using this equation, the stiffness matrix is found to be $\mathbf{K}^{ss} = \begin{bmatrix} 808.375 & -351.467 \\ -351.467 & 267.115 \end{bmatrix}$ kN/m.

Another similar static test was carried out for the TSM to validate the values of the stiffness matrix. By means of applying a static force P_1 at the rigid mass of the first floor, the displacement vector $\mathbf{x}^{ss} = [x_1, x_2]^T$ was determined (see Fig. 5.4b). The values of x_1 and x_2 obtained in this way were compared to those calculated with the following expression:

$$\mathbf{x}^{ss} = (\mathbf{K}^{ss})^{-1}\,\mathbf{P} \tag{5.4}$$

where $\mathbf{P}$ is the vector of external forces; in this case $\mathbf{P} = [P_1, 0]^T$.

Table 5.2 shows the comparison of the values of displacements x_1 and x_2, determined experimentally and numerically with Eq. (5.4). The accuracy is found to be acceptable.

The natural frequency of both bare frames were obtained numerically, i.e., $\omega = \sqrt{k/m}$ for the SSM (see Appendix B). In the case of the TSM it was necessary to solve the classical eingenvalue problem using matrices $\mathbf{M}^{ss}$ and $\mathbf{K}^{ss}$ [1, 61]. The theoretical results obtained in this way were compared to those got from the tests described in the next subsection.

5.2.2.4 Bare frame damping coefficients

Using white noise signals, the lateral frequencies of the bare frames, as well as their viscous damping coefficients, were determined by means of the spectra analyzer displayed in Fig. D.9 of Appendix D. Figs. 5.5 and 5.6 show the results of one test for the SSM and the TSM, respectively. In Tables 5.5 and 5.6 the results of all tests are registered. The boxes marked with '–' belong to illegible or out-of-range values. The values of the modal damping ratios, ξ, ξ_{br}, ξ_i and $(\xi_{br})_i$ were calculated by making the quotient of the real part between the imaginary part of the poles (see Figs. 5.5b and 5.6b) [64]. For example, from the output displayed in Fig. 5.5b, ξ is equal to $12.988 \times 10^{-3}/4.13487 = 0.003141$, and from the output shown in Fig. 5.6b, ξ_1 and ξ_2 are equal, respectively, to $15.3242 \times 10^{-3}/2.12532 = 0.007210$ and to $10.8929 \times 10^{-3}/6.38673 = 0.001706$.

For the SSM the damping coefficient was calculated using the well-known expression

$$c = 2\xi\sqrt{km} \tag{5.5}$$

In this case, $c = 2(0.003141)\sqrt{(334597)(533.5)} = 83.932$ N·s/m.

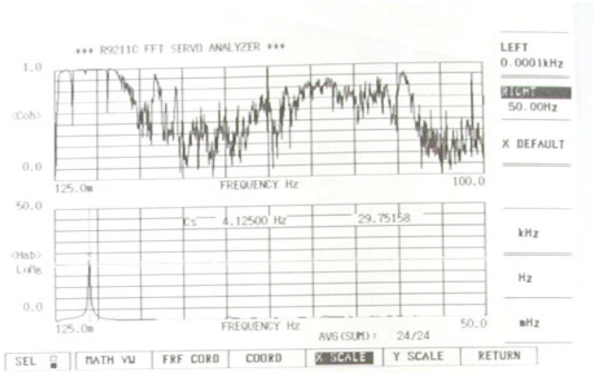

(a) Fundamental frequency of the bare frame

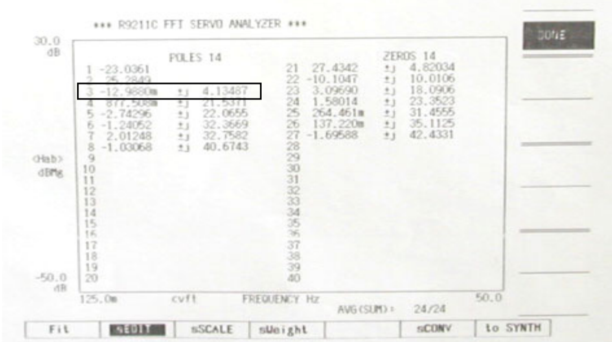

(b) Pole of the Fourier transformed used to calculate the damping ratio

Figure 5.5 Fundamental frequency obtained from a white noise signal

White noise test #	Bare frame		Braced frame	
	f (Hz)	ξ	f_{br} (Hz)	ξ_{br}
1	4.13487	0.003141	11.4784	0.059153
2	–	–	11.2716	0.070868
Average	**4.13487**	**0.003141**	**11.3750**	**0.065011**

Table 5.3 Modal parameters of the SSMFD

White noise	Bare frame				Braced frame			
test #	f_1 (Hz)	f_2 (Hz)	ξ_1	ξ_2	$(f_{br})_1$ (Hz)	$(f_{br})_2$ (Hz)	$(\xi_{br})_1$	$(\xi_{br})_2$
1	–	6.38608	0.001711	0.001565	4.88390	13.0433	0.069181	0.041096
2	2.14073	6.40858	0.001044	–	5.00995	13.1271	0.062126	–
3	2.12231	6.40603	0.008467	–	5.10354	13.7737	0.067881	0.034921
4	2.12532	6.38673	0.007210	0.001706	5.08378	–	0.065778	0.057066
Average	**2.12945**	**6.39686**	**0.004608**	**0.001636**	**5.02029**	**13.3147**	**0.066242**	**0.044361**

Table 5.4 Modal parameters of the TSMFD

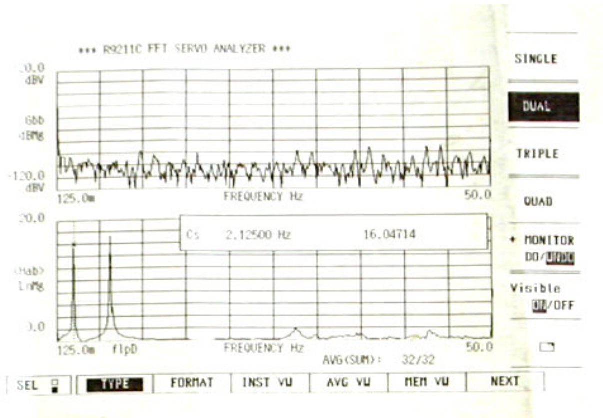

(a) Frequencies of the bare frame

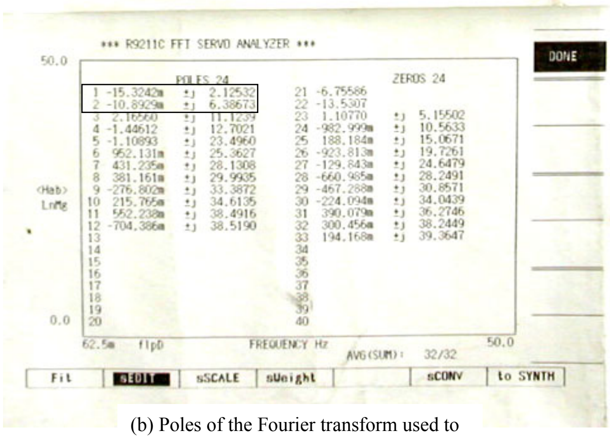

(b) Poles of the Fourier transform used to calculate the modal damping ratios

Figure 5.6 Frequencies of the TSM obtained from a white noise signal

For the TSM the damping matrix was determined applying the well-known expression

$$\mathbf{C}^{ss} = \left(\Phi^{-1}\right)^T \mathbf{C}^* \Phi^{-1} \tag{5.6}$$

where Φ is the mode shape matrix. Knowing $\mathbf{M}^{ss}$ and $\mathbf{K}^{ss}$ it is possible to obtain Φ by means of a classical modal analysis [1, 61]. In this case, the mode shape matrix is $\Phi = \begin{bmatrix} 0.588513 & 1.221430 \\ 1.200240 & -0.578306 \end{bmatrix}$. $\mathbf{C}^*$ is the modal damping matrix:

$$\mathbf{C}^* = \begin{bmatrix} 2\xi_1\omega_1 m_1 & 0 \\ 0 & 2\xi_2\omega_2 m_2 \end{bmatrix} \tag{5.7}$$

where $\omega_1 = 2\pi f_1 = 13.3797$ rad/s, $\omega_2 = 2\pi f_2 = 40.1927$ rad/s (see Table 5.4 for values of f_1 and f_2). Substituting these values in Eq. (5.7), $\mathbf{C}^* = \begin{bmatrix} 0.120714 & 0 \\ 0 & 0.139864 \end{bmatrix}$. Now, applying Eq. (5.6), the damping matrix of the bare frame is found to be $\mathbf{C}^{ss} = \begin{bmatrix} 72.692 & -4.065 \\ -4.065 & 68.688 \end{bmatrix}$ N·s/m.

5.2.2.5 Bracing and FD masses

For both models, the SSM and the TSM, mass m' and matrix $\mathbf{M}^{dd}$ were neglected. This assumption relies on the comparison between numerical an experimental results.

5.2.2.6 Bracing stiffness coefficients

The stiffness coefficients of the braces cannot be obtained from theoretical considerations due to the difficulties in evaluating the axial stiffness of the braces as load-cells were connected to them (see Fig. D.5). Thus, the corresponding values of both the bare and the braced frame were used to calculate these stiffness coefficients.

For the SSMFD, the bracing stiffness k' was determined applying

$$k' = k_{br} - k \tag{5.8}$$

where k is the bare frame stiffness and k_{br} is the braced frame stiffness. This last value was calculated with the following expression:

$$k_{br} = 4\pi^2 f_{br}^2 m \tag{5.9}$$

The values of f_{br} and m, are, respectively, 11.375 Hz (see Table 5.3) and 533.5 kg.

Main frame (average values)	Bracing system + FD (average values)
$m = 533.5$ kg	$m' = 0$
$c = 83.932$ N·s/m ($\xi = 0.003141$)	$c' = 0.0$ ($\xi' = 0.0$)
$k = 334.597$ kN/m	$k' = 2390.596$ kN/m
$T = 0.2509$ s	

Table 5.5 Dynamic parameters of the SSMFD

For the TSMFD, the stiffness matrix of the bracing, $\mathbf{K}^{dd}$, was calculated applying

$$\mathbf{K}^{dd} = \mathbf{K}^{br} - \mathbf{K}^{ss} \tag{5.10}$$

where $\mathbf{K}^{ss}$ is stiffness matrix of the bare frame and $\mathbf{K}^{br}$ is the stiffness matrix of the braced frame. This latter was determined applying the following expression

$$\left|\mathbf{K}^{br} - (\omega_{br})_i^2 \, \mathbf{M}^{br}\right| = 0 \tag{5.11}$$

where $(\omega_{br})_1^2 = 4\pi^2 \left(f_{br}\right)_1^2$ and $(\omega_{br})_2^2 = 4\pi^2 \left(f_{br}\right)_2^2$. The values of $\left(f_{br}\right)_1$ and $\left(f_{br}\right)_2$ are, respectively, 5.02029 Hz and 13.3147 Hz (see Table 5.4). $\mathbf{M}^{br}$ is the mass matrix of the braced frame (the values of this matrix are considered equal to those of $\mathbf{M}^{ss}$: $\mathbf{M}^{br} = \begin{bmatrix} 533.5 & 0 \\ 0 & 552.5 \end{bmatrix}$ kg as the masses of the bracing system are neglected). Taking into account the special form of matrix $\mathbf{K}^{dd}$ and performing an iterative calculation, matrix $\mathbf{K}^{br}$ was found to be $\mathbf{K}^{br} = \begin{bmatrix} 3071.160 & -1320.382 \\ -1320.382 & 1236.026 \end{bmatrix}$ kN/m.

Now, applying Eq. (5.10), $\mathbf{K}^{dd}$ was found to be $\mathbf{K}^{dd} = \begin{bmatrix} 2262.777 & -968.889 \\ -968.889 & 968.889 \end{bmatrix}$ kN/m

5.2.2.7 Bracing damping coefficients

For both models, the SSM and the TSM, damping c' and the components of damping matrix $\mathbf{C}^{dd}$ were neglected.

5.2.2.8 Summary

Tables 5.5 and 5.6 summarize the dynamic parameters of the SSMFD and the TSMFD, respectively.

Main frame (average values)	Bracing system + FD (average values)
$\mathbf{M}^{ss} = \begin{bmatrix} 533.5 & 0 \\ 0 & 552.5 \end{bmatrix}$ kg	$\mathbf{M}^{dd} = \begin{bmatrix} 0 & 0 \\ 0 & 0 \end{bmatrix}$
$\mathbf{C}^{ss} = \begin{bmatrix} 72.692 & -4.065 \\ -4.065 & 68.688 \end{bmatrix}$ N·s/m	$\mathbf{C}^{dd} = \begin{bmatrix} 0 & 0 \\ 0 & 0 \end{bmatrix}$
$\mathbf{K}^{ss} = \begin{bmatrix} 808.375 & -351.467 \\ -351.467 & 267.115 \end{bmatrix}$ kN/m	$\mathbf{K}^{dd} = \begin{bmatrix} 2262.777 & -968.889 \\ -968.889 & 968.889 \end{bmatrix}$ kN/m
$\mathbf{T}^{ss} = \begin{bmatrix} 0.4797 \\ 0.1470 \end{bmatrix}$ s	

Table 5.6 Dynamic parameters of the TSMFD

5.3 Friction Dissipators

5.3.1 Description

All the friction dissipators are alike. They consist of a hollow block of stainless steel with a cut along its length. The hole is a cylinder whose axis goes along the length of the block. This hole holds the brace. Two smaller holes were drilled to hold two adjustable bolts to control the prestressing normal force between the FD and the brace. Fig. 5.7 shows a detail of the FD and Fig. 5.8 displays a picture of an actual FD.

5.3.2 Numerical modelling

In order to determine a relationship between the applied torque and the prestressing force in the friction dissipator, this was tested under tension and compression loads. This fact was accounted for in the numerical simulations. The results are shown in Fig. 5.9. It can be seen that the behavior of the FD under compression and tension loads is not regular.

For the numerical simulations, however, the values of the sliding loads were identified, for each test, by observing the output.

5.4 Tests

5.4.1 Description

The tests consisted in applying seismic inputs to each model. The information regarding the input signals and the totality of the obtained results, can be found in Appendix E.

Both models, the SSBFD and the SSMFD were instrumented (see Figs. D.5 and D.6 of Appendix D) to obtain the displacements and accelerations of the floors. Other measured parameters were: the friction force F_i^{FD} and the sliding displacement x_i^{FD} (see Figs. 5.10 and 5.11). Since these two values were measured along the brace axis, the horizontal projections of these quantities were calculated applying the following expressions:

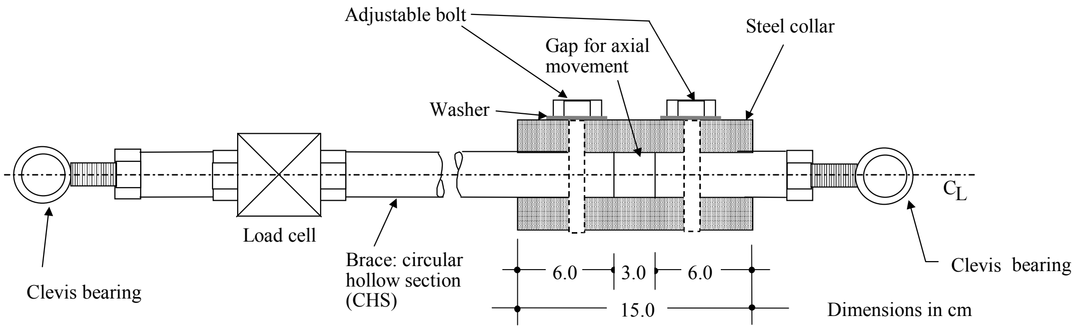

(a) FD-brace connection

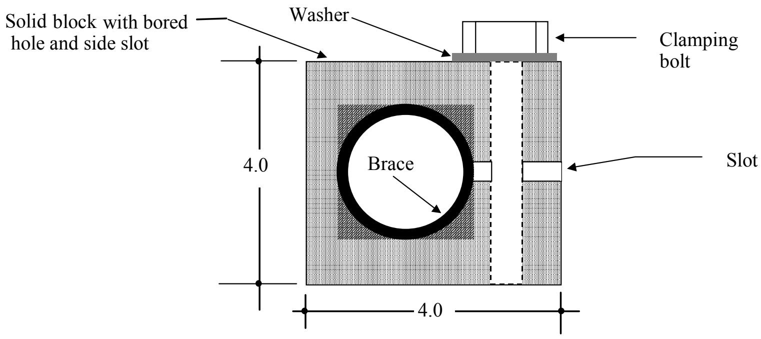

(b) FDCross section

Figure 5.7 Detail of the FD-brace connection

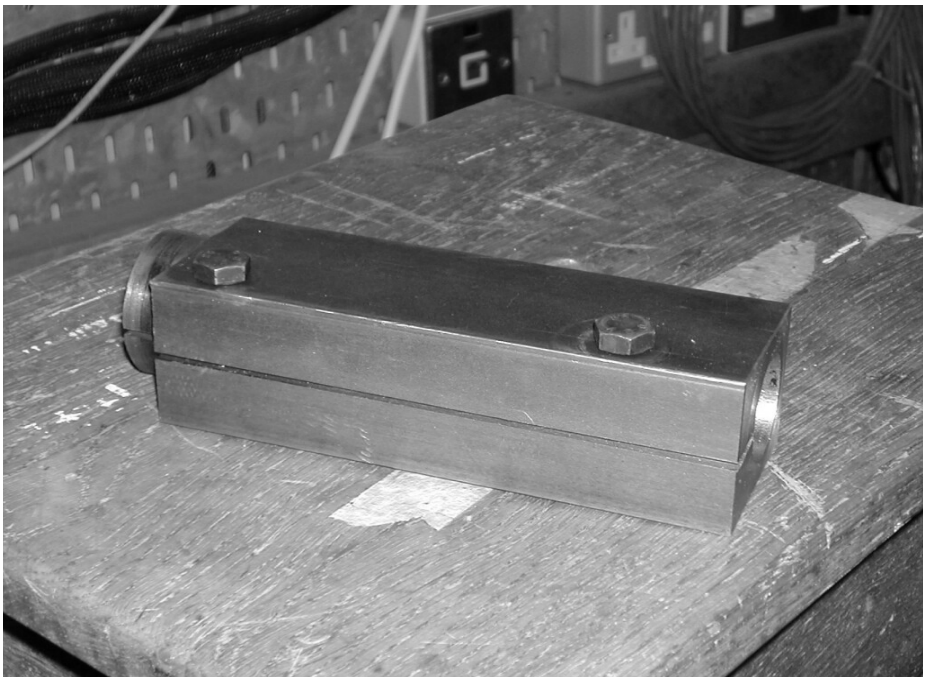

Figure 5.8 Metallic FD used in the tests

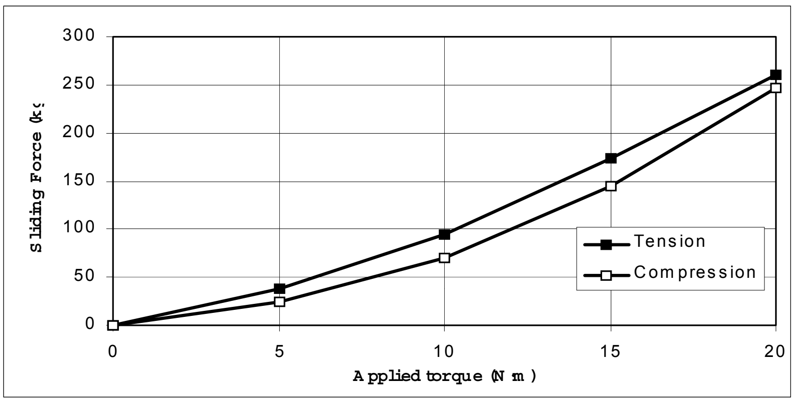

Figure 5.9 Sliding force of a FD, obtained with a compression and tension test

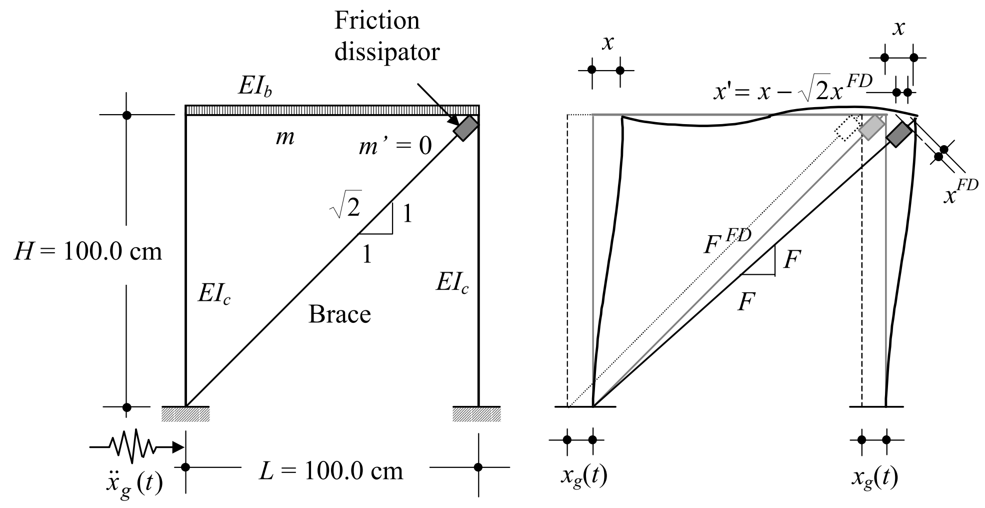

(a) Single-story model with a friction dissipator (SSMFD)

(b) Assumed motions of the main structure and the friction dissipator

Figure 5.10 Horizontal motion of the SSBFD

$$F_i = F_i^{FD}/\sqrt{2} \quad \text{(horizontal projection of friction force)} \tag{5.12}$$

$$\left(x_i - x_i'\right) = \sqrt{2}x_i^{FD} \quad \text{(horizontal projection of relative displacement)} \tag{5.13}$$

These horizontal projections are used to draw the plots shown in this section and in Appendix E.

5.4.2 Single-story model with a friction dissipator (SSMFD)

5.4.2.1 Response to a sine-dwell

The sine-dwell depicted in Fig. 5.12 was applied to the shaking-table to obtain the response of the SSFBD. The sine-dwell is a sine signal which has a constant frequency of 25.1327 rad/s (4 Hz). Note that this frequency is close to the natural frequency of the bare frame, 4.1349 Hz (see Table 5.3). The amplitude of the signal varies from 0 to a maximum value of $PGA = 0.30g$.

In Fig. 5.13 the displacement responses of the SSBFD, $x - t$, and of the FD, $x' - t$, are depicted. The black line corresponds to the main frame displacement, x, and the grey line corresponds to the dissipator displacement, x'.

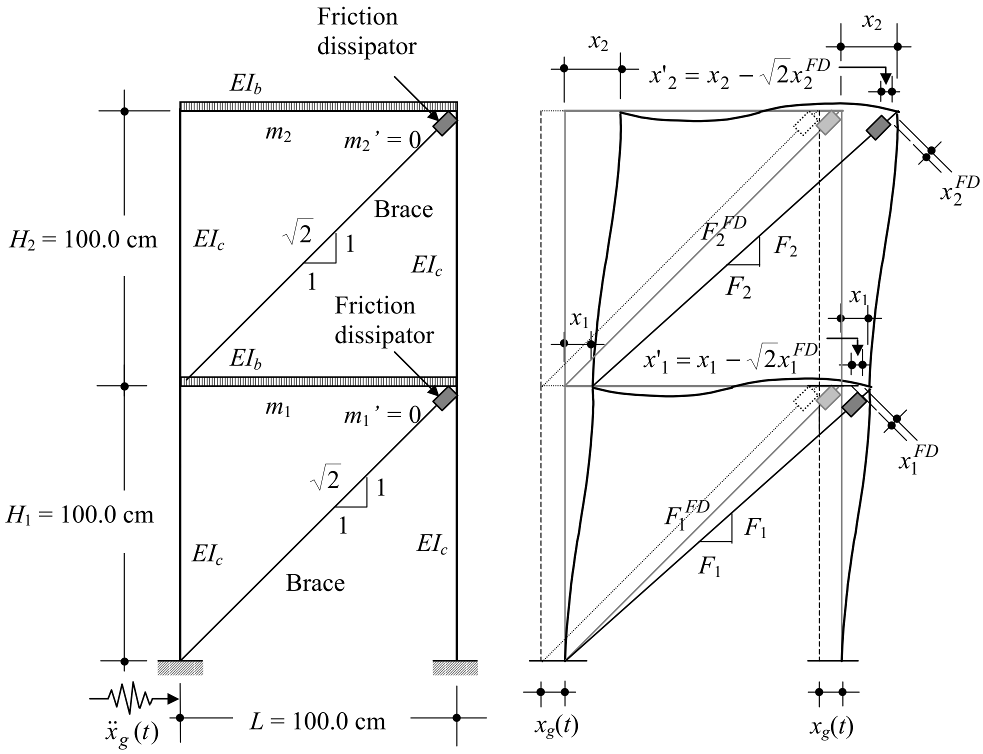

(a) Two-story model with friction dissipators (TSMFD)

(b) Assumed motions of the main structure and the friction dissipators

Figure 5.11 Horizontal motion of the TMSFD

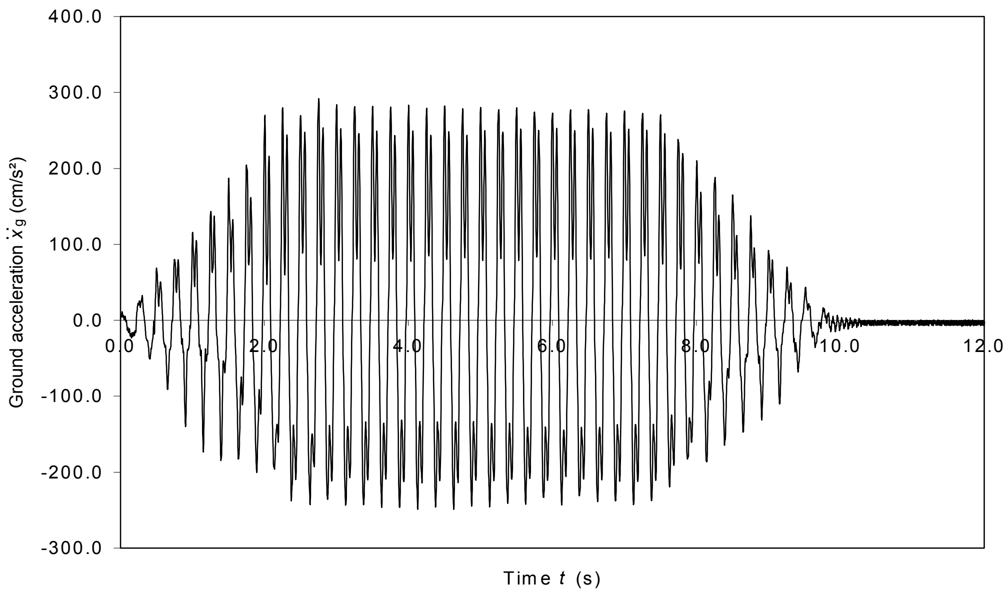

Figure 5.12 Sine-dwell signal (frequency = 4 Hz)

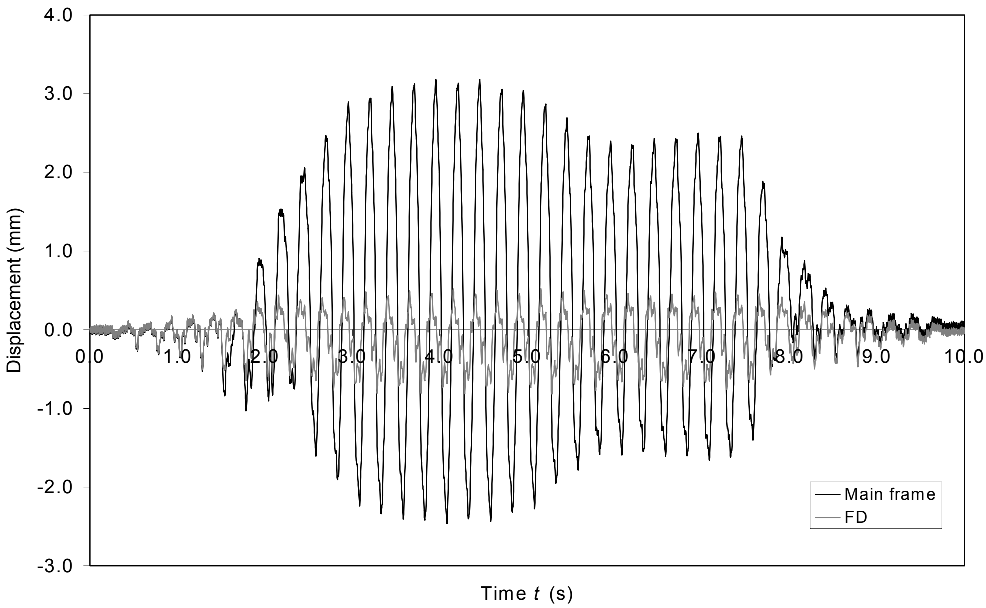

Figure 5.13 Response of the SSMFD subjected to a sine-dwell acceleration

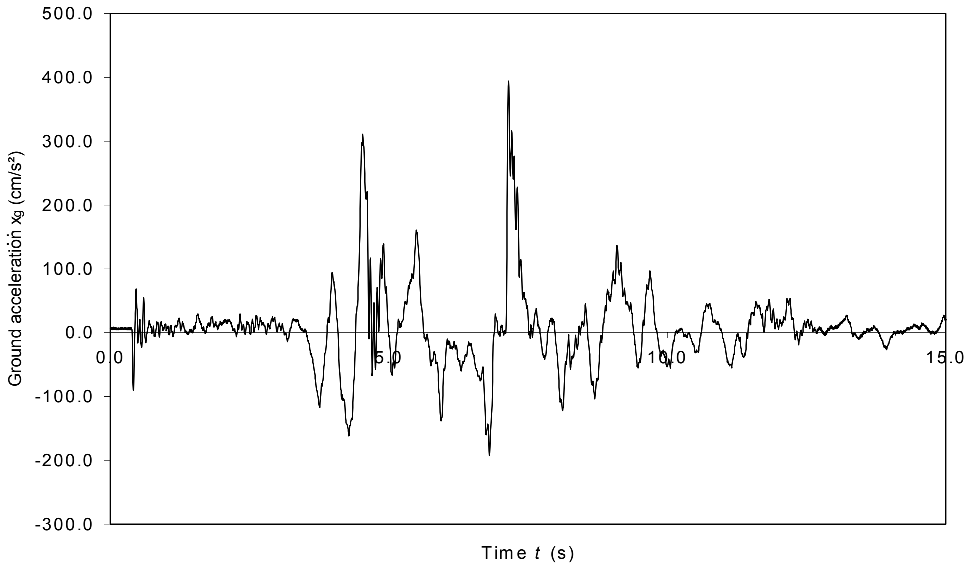

Figure 5.14 Northridge earthquake (January 17, 1994, 90°)

5.4.2.2 Response to the Northridge earthquake

The ground acceleration depicted in Fig. 5.14 was applied to the shaking-table to obtain the response of the SSFBD. The $PGA = 0.40g$ in this case.

In Fig. 5.15 the displacement responses of the SSBFD and the FD are depicted. The black line shows the main frame displacement, x, and the grey line corresponds to the dissipator response, x'.

5.4.3 Two-story model with friction dissipators (TSMFD)

5.4.3.1 Response to the Northridge earthquake

The ground acceleration depicted in Fig. 5.14, scaled by a factor of 0.60, was applied to the shaking-table to obtain the response of the TSMFD. The $PGA = 0.24g$ in this case.

The displacement responses of the first and the second floor are plotted in Figs. 5.16 and 5.17, respectively. The black line corresponds to the main frame displacement, x_i and the grey line belongs to the dissipator displacement, x'_i.

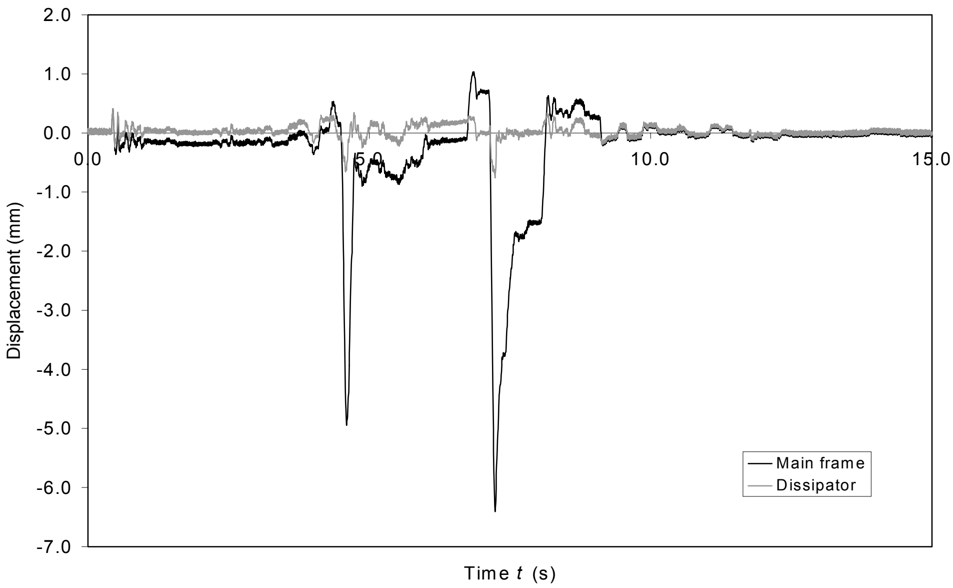

Figure 5.15 Response of the SSMFD for the Northridge earthquake

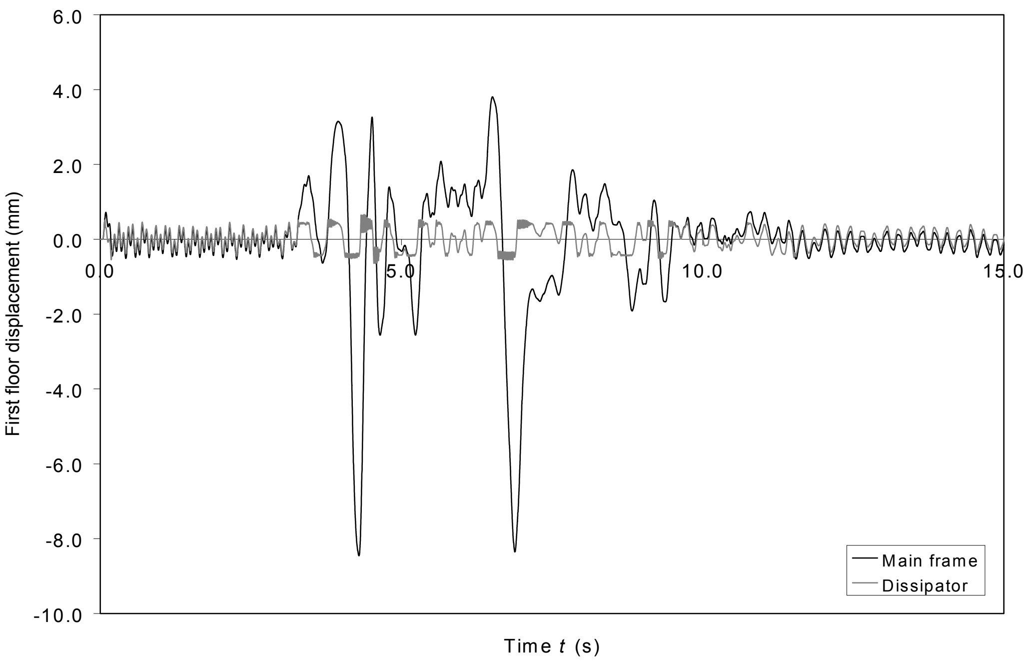

Figure 5.16 First floor response of the TSMFD for the Northridge earthquake

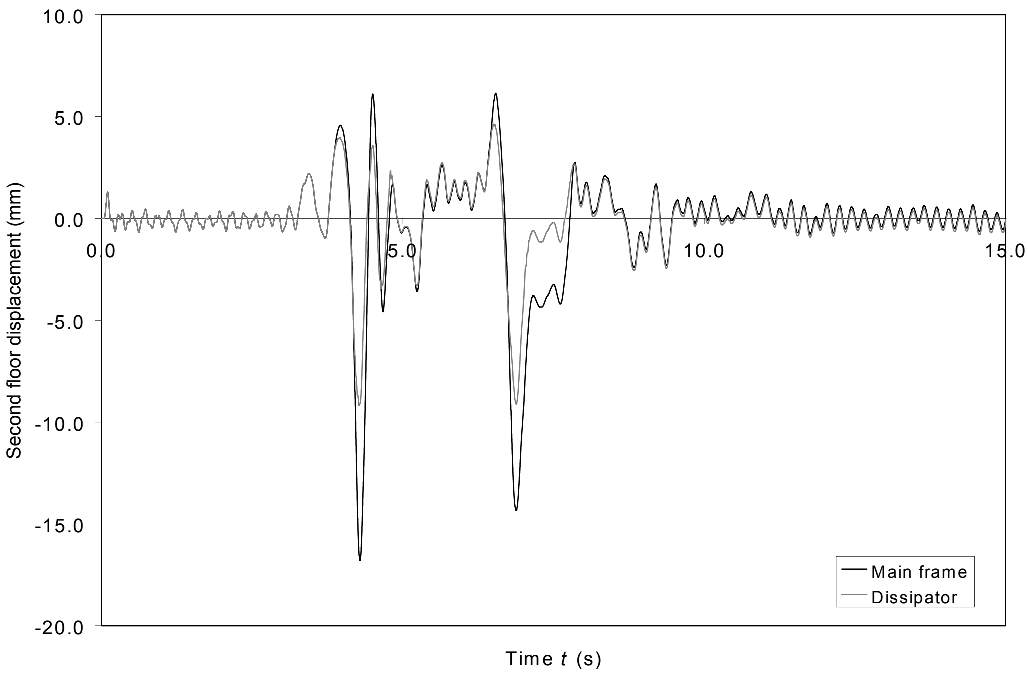

Figure 5.17 Second floor response of the TSMFD for the Northridge earthquake

5.5 Comparison between Experimental and Numerical Results

5.5.1 SSMFD

For the case of the sine-dwell depicted in Fig. 5.12, the displacement time-history of the SSMFD (see Fig. 5.13), is compared to the one obtained with ALMA (see Fig. 5.18). The difference between the responses is due possible to the difficulties to reproduce the non-linear behavior near resonance.

Also for this input, the relationships $F-(x-x')$ for the tests and ALMA are depicted in Fig. 5.19. The positive values of F correspond to tension forces and the negative values correspond to compression forces. The differences between Figs. 5.18a and b and between Figs. 5.19a and b suggest that under harmonic driving forces whose frequency are close to that of the bare frame, the dynamic behavior of FD cannot be modelled numerically taking into account the established principles of Coulomb's dry friction (see Sect. 2.1).

For the Northridge earthquake, the comparison between experimental and numerical responses is shown in Fig. 5.20, and in Fig. 5.21 the experimental and numerical hysteresis loops (relationship $F-(x-x')$) are plotted. Figs. 5.20 and 5.21 indicate the acceptable accuracy of the numerical model when getting the dynamic response of SSBFD subjected to earthquake loads.

5.5.2 TSMFD

For the case of seismic input depicted in Fig. 5.14, the displacement time-histories of the TSMFD, obtained from ALMA and from the tests, are shown in Figs. 5.22 (first floor) and 5.25 (second floor), respectively. The black line corresponds to the response obtained with ALMA, and the grey line corresponds to the response obtained from the tests. For the case of the main frame (see Figs. 5.22a and 5.24a), the responses are very close each other. On the other hand, for the FDs, Figs. 5.22b and 5.24b show differences which indicate the difficulty to model numerically the dynamic behavior of these devices.

Relationships $F-(x-x')$ for the first and second floor are plotted, respectively, in Figs. 5.23 and 5.25. Figs. 5.23a and 5.25a depict the hysteresis loops obtained experimentally and Figs. 5.23b and 5.25b show the hysteresis loops obtained using ALMA. The similarities between the hysteresis loops in each floor is clear.

5.6 Summary

A series of shaking-table tests on two reduced-scale models was described in this chapter. The dynamic response obtained with the tests for a number of seismic inputs was presented. The results obtained with the tests were compared to the results obtained using ALMA. The responses are very close each other, which indicates that ALMA is a good numerical procedure to obtain the dynamic response of buildings equipped with friction dissipators.

On the other hand, Figs. 5.23a and 5.25a show that the FD did not follow the dry friction principles. Hence, this situation cannot be accurately reproduced with ALMA. Even so, the numerical and experimental displacement time-histories of the main frame (Figs. 5.22a and 5.24a) are quite similar.

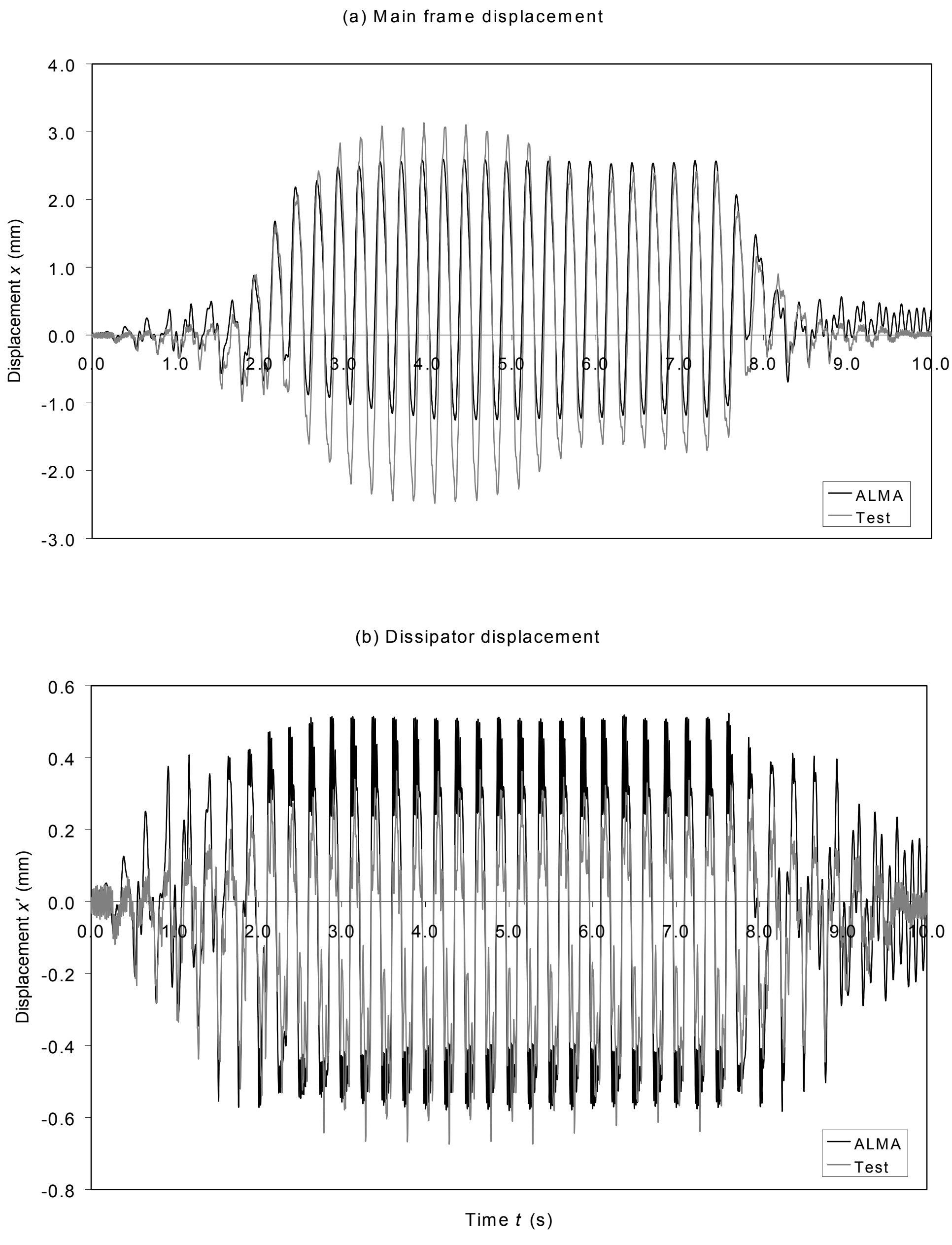

Figure 5.18 Comparison between the SSBFD displacements from ALMA and from testing for the sine-dwell signal

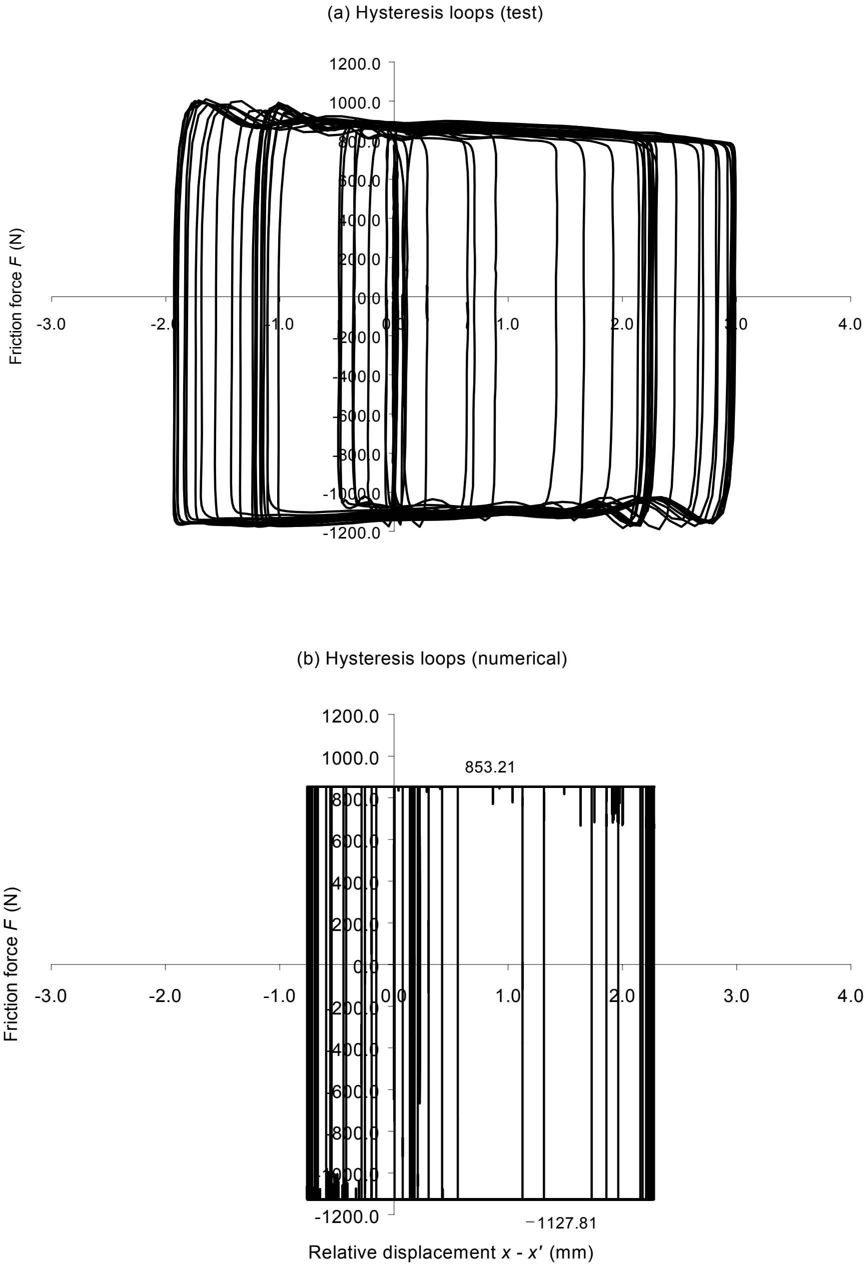

Figure 5.19 Comparison between the SSBFD hysteresis loops from ALMA and from testing for the sine-dwell signal

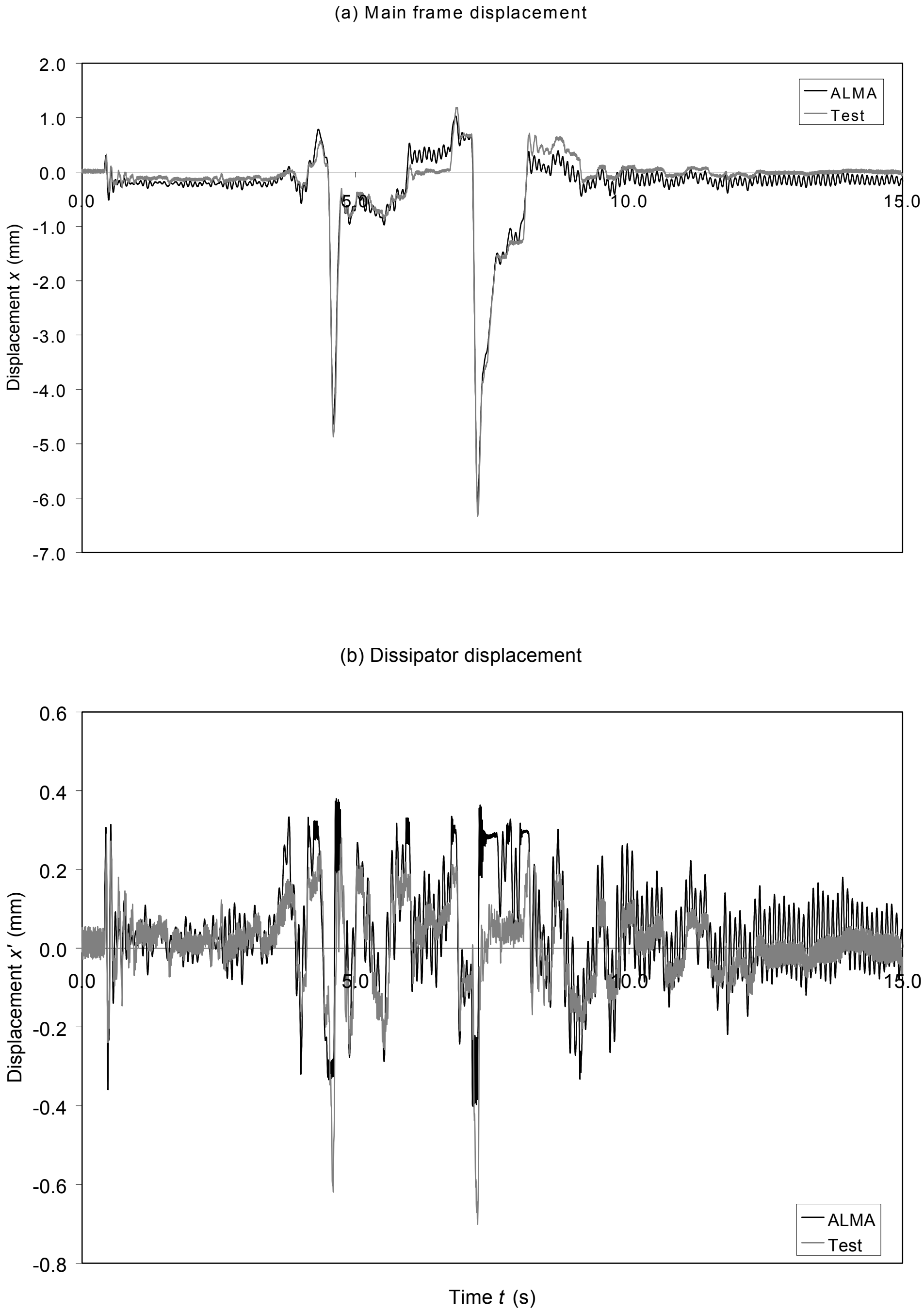

Figure 5.20 Comparison between the SSBFD displacements from ALMA and from testing for the Northridge earthquake

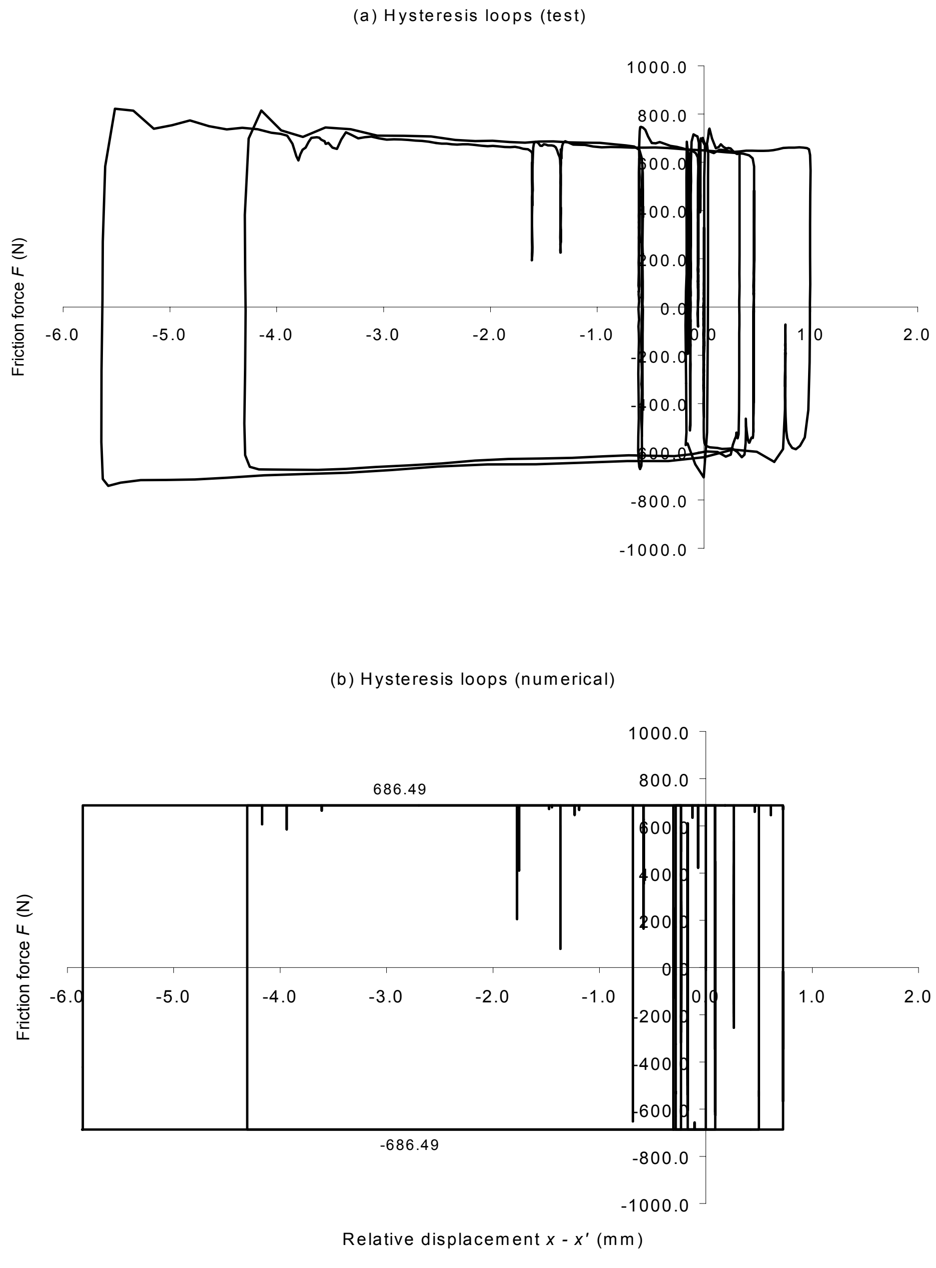

Figure 5.21 Comparison of the SSBFD hysteresis loops from ALMA and from testing for the Northridge earthquake

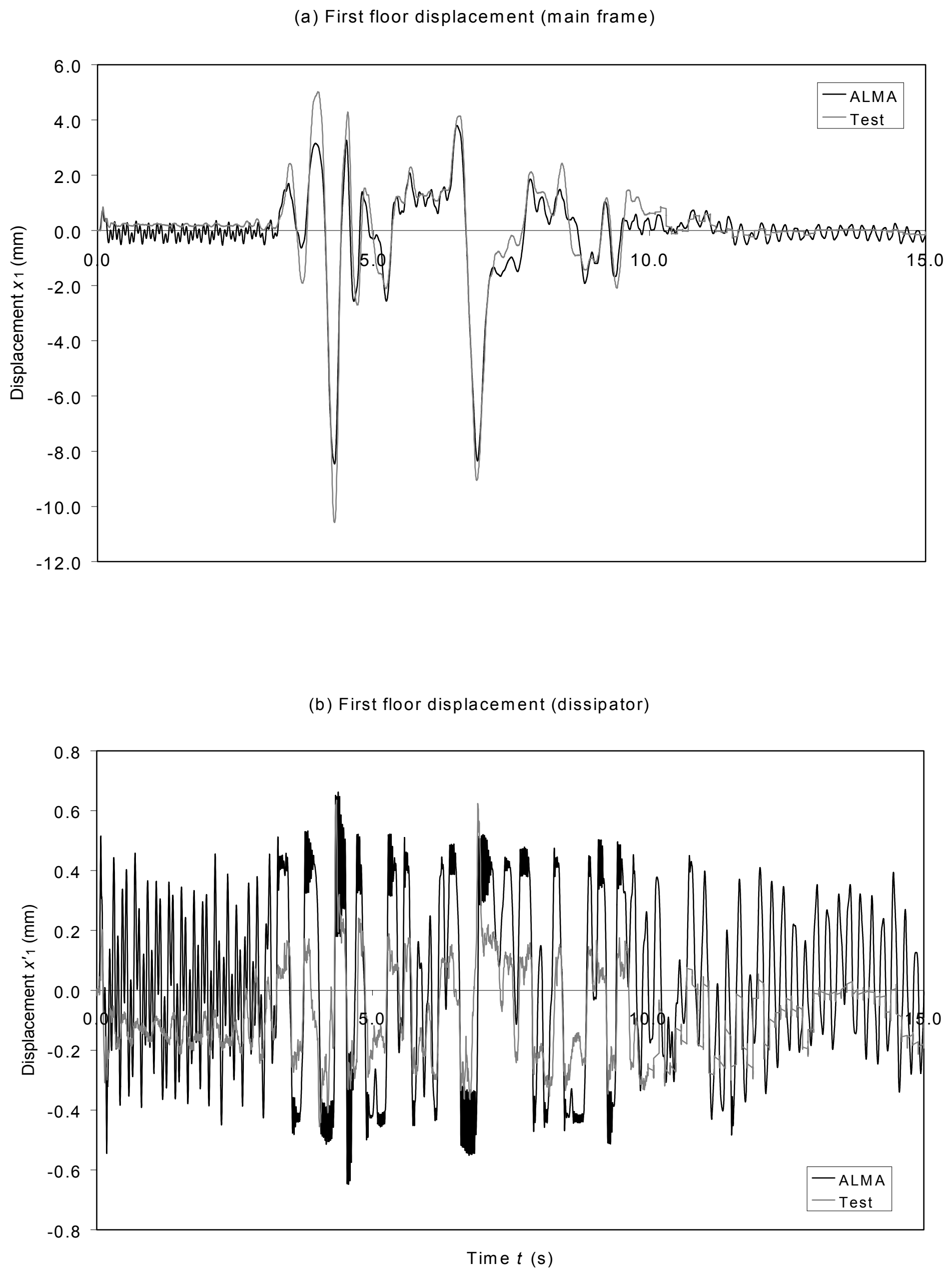

Figure 5.22 Comparison between the first floor displacements from ALMA and from testing for the Northridge earthquake

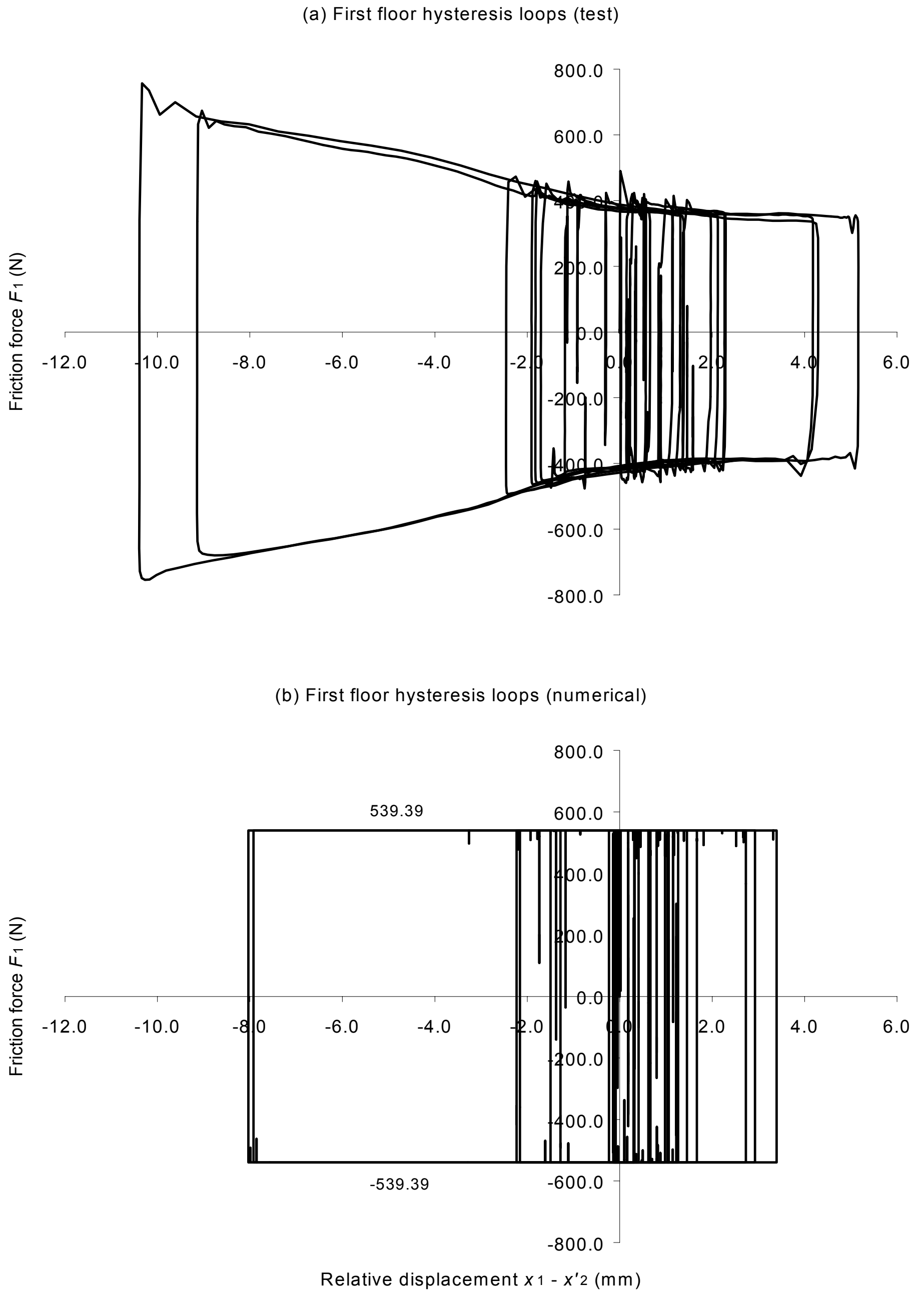

Figure 5.23 Comparison between the first floor hysteresis loops obtained from ALMA and from the tests for the Northridge earthquake

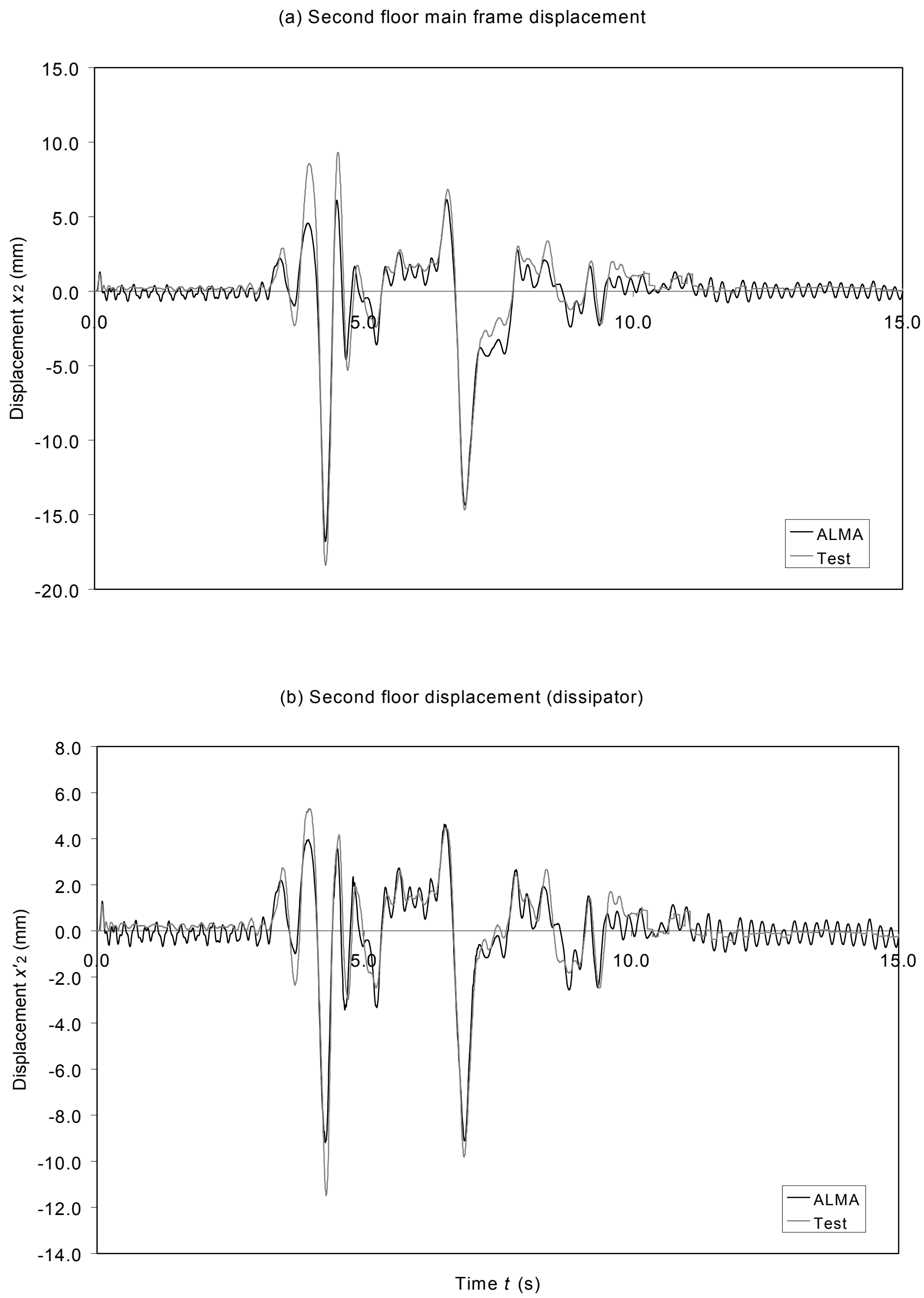

Figure 5.24 Comparison between the second floor displacements from ALMA and from testing for the Northridge earthquake

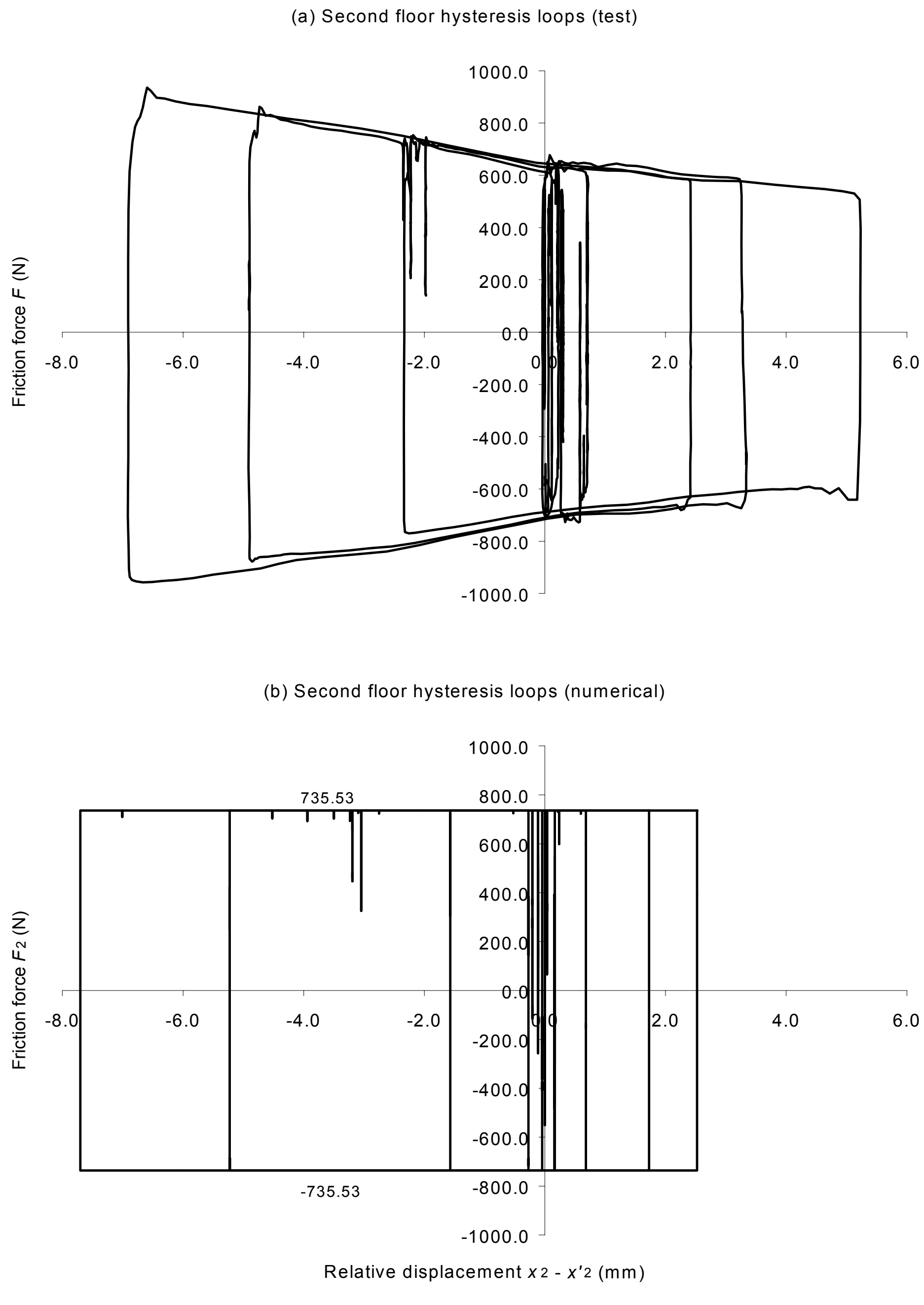

Figure 5.25 Comparison between the second floor hysteresis loops from ALMA and from testing for the Northridge earthquake